Polymer Chemistry

ROYAL SOCIETY OF CHEMISTRY

PAPER

View Article Online
View Journal

Cite this: DOI: 10.1039/d5py00552c

Halochromic oxazolidine nanofibers as portable smart chemosensors for dual-mode colorimetric and fluorimetric detection of food spoilage: investigation of solid-state pH responsivity in polar microenvironments†

Bahareh Razavi [a] and Babak Karimi *[a,b]

Received 4th June 2025,
Accepted 7th July 2025

DOI: 10.1039/d5py00552c

rsc.li/polymers

Today, the world increasingly depends on smart technologies, particularly in the realm of food safety. Among these innovations, one of the most significant solutions for addressing the challenges of timely and efficient visual detection of food spoilage is the use of intelligent tags in food packaging. In this study, an innovative class of intelligent sensors based on halochromic oxazolidine (hydroxyl and tertiary amine-functionalized) nanofibers was developed by electrospinning of functionalized copolymers based on methyl methacrylate (MMA) and functional comonomers that have various polar groups, including tertiary amine, sulfonic acid, and hydroxyl groups. Hence, the pH responsiveness of oxazolidine derivatives was examined across a pH range from 1 to 14, and in the presence of various types of aliphatic and aromatic amines, the most significant alkaline products generated during food spoilage. The pH responsiveness of halochromic nanofibers is primarily influenced by interactions between the functional groups of oxazolidine molecules and the polymer matrix, along with solvatochromic behavior, which together enable the fibers to change color in response to pH variations. Therefore, three pH-responsive sensor tags based on halochromic nanofibers were designed for precise and timely spoilage detection in milk, lamb, chicken, and fish foods by dual-mode fluorimetric and colorimetric monitoring of acidic and basic vapors by the protonation and deprotonation of oxazolidine molecules. The intelligent pH-indicator nanofibers effectively detected spoilage in milk, lamb, and chicken meat within 3 days, and in fish within 2 days, highlighting their potential for developing wireless, selective optical chemosensors responsive to microenvironmental polarity changes.

1. Introduction

Food spoilage, especially in protein-rich products, is a big challenge for food safety, public health, and the economy. Spoilage not only leads to the loss of valuable food but also increases the risk of foodborne illnesses because harmful microorganisms and toxins can develop. To solve these problems, we need new methods that can both accurately detect and effectively prevent spoilage. During spoilage, many foods, especially those that break down through enzymatic processes, release acidic vapors. Dairy products, for example, release these vapors due to lactic acid fermentation by lactic acid bacteria. These bacteria convert lactose (milk sugar) into lactic acid, which causes the sour taste and lowers the pH, signaling spoilage.[1–5] Conversely, foods that undergo spoilage due to protein breakdown, such as seafood and certain meats, can release basic compounds like ammonia (NH_3) and organic amines. Ammonia is formed as a result of microbial metabolism and the enzymatic breakdown of nitrogenous compounds present in these foods. In this context, an indicator that can detect pH fluctuations in the medium becomes essential for applications in the food industry.[6–9]

Among the different types of stimuli-responsive organic molecules, halochromic oxazolidine derivatives with a range of

[a]Department of Chemistry, Institute for Advanced Studies in Basic Sciences (IASBS), Prof. Yousef Sobouti Boulevard, Zanjan, 45137-66731, Iran
[b]Research Center for Basic Sciences & Modern Technologies (RBST), Institute for Advanced Studies in Basic Sciences (IASBS), Prof. Yousef Sobouti Boulevard, Zanjan, 45137-66731, Iran. E-mail: karimi@iasbs.ac.ir, bkarimi48@gmail.com

†Electronic supplementary information (ESI) available: Materials, typical procedures for the synthesis of multi-functionalized copolymer nanoparticles and also synthesis of oxazolidine derivatives, ^{1}HNMR and ATR-FTIR spectra, DLS curves, and FESEM images for latex nanoparticles, the adsorption isotherm diagram in BET analysis for nanofibers, AFM results for nanofibers containing oxazolidine, the kinetics study of pH changes as a function of time used for detection of milk spoilage. See DOI: https://doi.org/10.1039/d5py00552c

functional groups have attracted considerable interest. Their ability to undergo color changes and emit fluorescence in response to pH variations makes them especially valuable for various applications.[10–14] These derivatives are highly effective at indicating pH changes, making them essential for monitoring both chemical and biological processes. The physical interaction between oxazolidine and its surrounding environment results in solvatochromic behavior. This color shift occurs due to changes in the molecule's electronic structure, which in turn influence its light absorption and emission properties. Additionally, the halochromic color change of oxazolidine is often reversible, allowing the material to return to its original color once the pH is restored to neutral.[15–17] This makes halochromic oxazolidine derivatives a valuable tool for applications that require real-time pH monitoring, such as food safety, environmental monitoring, and healthcare diagnostics. However, due to their limited optical properties in solution, these small molecules should be integrated into a polymer matrix to enhance their performance.

Nanofibers are a promising option in the field of intelligent polymers for detecting food spoilage. These nanoscale fibers possess unique properties that make them well-suited for sensing applications.[18–20] In the context of food spoilage detection, nanofibers can be functionalized with specific groups that interact with target molecules, such as volatile organic compounds (VOCs), which are released during spoilage.[21–23] By incorporating halochromic oxazolidine compounds into the nanofiber matrix, the nanofibers can selectively capture and detect spoilage indicators, triggering a measurable response. The polar functional groups in the nanofibers improve their sensitivity to target molecules, allowing for the rapid and precise detection of even trace amounts of spoilage markers. This is due to both their interaction with oxazolidine functional groups and the pH changes in the surrounding medium. Moreover, the flexibility and versatility of nanofibers make them suitable for integration into various packaging materials, enabling continuous monitoring throughout the storage and transport of food products. Their reusability and reversibility further enhance their practical utility, as the nanofibers can be used multiple times without degrading their optical performance.[24–26] By carefully selecting the appropriate method for incorporating oxazolidine into the nanofiber matrix, the optical properties of the halochromic compound can be optimized, thereby improving its effectiveness in detecting food spoilage. For this purpose, oxazolidine can be integrated into the nanofiber matrix during the electrospinning process.[27,28] The spinning process creates a microenvironment around the oxazolidine molecules, which enhances their optical properties by limiting their movement and preventing aggregation. These intelligent copolymer nanofibers are advanced materials that can undergo reversible property changes when exposed to external stimuli, such as pH fluctuations or the presence of specific molecules.[29–32] Smart polymers can be incorporated into food packaging materials to create intelligent packaging systems. These smart nanofibers can be embedded in packaging films or applied directly to food surfaces. When spoilage occurs, the nanofibers respond by triggering detectable changes in their properties, such as color shifts, variations in fluorescence intensity, or even fluorescence quenching. These changes can be easily monitored using solid-state UV-Vis and fluorescence spectroscopy.[33–38]

In this study, multifunctional polymer nanoparticles were synthesized *via* emulsion copolymerization of methyl methacrylate (MMA) with functional monomers, including hydroxyethyl methacrylate (HEMA), dimethylaminoethyl methacrylate (DMAEMA), and 2-acrylamido-2-methylpropanesulfonic acid (APSA), at a concentration of 20 wt% relative to the total polymer content. Additionally, two oxazolidine derivatives, each containing hydroxyl and tertiary amine functional groups, were synthesized and characterized to serve as halochromic indicators for pH detection. The halochromic oxazolidine dye was incorporated into the copolymer solution during the pre-electrospinning stage, ensuring its inclusion in the nanofibers as they formed. The functional groups in the nanofibers influenced their diameter, surface chemistry, and topology, which, in turn, impacted their ability to adsorb vapors released during food spoilage. The pH-responsive behavior of the resulting stimuli-responsive nanofibers was assessed using solid-state UV-Vis and fluorescence spectroscopy to study the solvatochromic properties of the oxazolidine molecules when exposed to acidic and basic environments. These smart nanofibers were used to detect food spoilage at room temperature over a five-day period, with sensor tags providing visual alerts *via* colorimetric or fluorimetric changes, triggered by acidic or basic vapors produced during spoilage through protonation and deprotonation of the oxazolidine molecules. Furthermore, the reusability of these smart nanofiber tags was evaluated, demonstrating their potential for multiple applications.

2. Experimental section

2.1. Materials

DMAEMA, MMA, HEMA, 2-acrylamido-2-methylpropanesulfonic acid (APSA), sodium dodecyl sulfate (SDS), anhydrous magnesium sulfate ($MgSO_4$), potassium persulfate (KPS), Triton X-100, glacial acetic acid, sodium hydrogen carbonate ($NaHCO_3$), and all of the solvents were supplied by Merck Chemical Company. The raw materials required for the synthesis of (*E*)-4-(2-(9,9-dimethyl-2,3-dihydrooxazolo[3,2-*a*]indol-9a(9*H*)-yl)vinyl) phenol (OXOH) and (*E*)-2-(4-(dimethylamino)styryl)-3-(2-hydroxyethyl)-1,1-dimethyl-1*H*-benzo[*e*]indol-3-ium including 1,1,2-trimethylbenz[*e*]indole (98%), 2-bromoethanol (95%), 4-hydroxybenzaldehyde (98%), and 4-dimethylaminobenzaldehyde (98%) were purchased from Sigma-Aldrich. Distilled deionized (DI) water was used in all of the recipes, and all of the materials were used without further purification. To investigate food spoilage processes, we used dairy and protein-rich foods, including pasteurized milk, lamb meat, fish (farmed trout), and chicken meat. All fresh food samples were randomly purchased from the local market in Zanjan, Iran, for the spoilage experiments. The samples were stored in an ice chest and transported to the lab-

oratory, where they were immediately analyzed upon arrival. The meat samples (chicken and lamb) were carefully selected from lean, fat-free sections, and all protein samples, including chicken, lamb, and fish, were aseptically cut into small portions. The pasteurized milk used in this study had a shelf life of 9 days when stored at refrigeration temperature (4 ± 1 °C) and was used fresh at room temperature immediately after purchase for the milk spoilage experiment.

2.2. Synthesis of multi-functionalized copolymer nanoparticles

Multifunctional poly(methyl methacrylate) copolymer nanoparticles (PM-NPs), containing approximately 10 wt% solid content, were synthesized through the emulsion copolymerization of MMA with various acrylate and methacrylate functional monomers, including DMAEMA (PMDM-NPs), HEMA (PMHE-NPs), and APSA (PMSO-NPs), each comprising approximately 20 wt% relative to the total solid polymer, as detailed in Table 1. The synthesis was carried out in four naked glass reactors, each equipped with a mechanical stirrer, condenser, and dropping funnel. The reactors were initially maintained at 25 °C, where a mixture of water, $NaHCO_3$, sodium dodecyl sulfate (SDS), and Triton X-100 was added and stirred at 100 rpm for 30 minutes. Subsequently, a pre-emulsified solution was prepared by gradually adding a monomer mixture (MMA and a secondary monomer) to the reactors at a controlled rate of one drop per second. Following this, a 5 ml KPS solution was slowly introduced into the mixture while maintaining the temperature at 25 °C with continued stirring for 20 minutes. The temperature was then elevated to 80 °C, and the stirring speed was increased to 200 rpm to initiate the copolymerization reaction, which was sustained for 3 hours to ensure the process reached completion. Monomer conversion and the final solid content of each sample were evaluated using gravimetric analysis, with the results provided in Table 1.

2.3. Synthesis of oxazolidine derivatives

The synthesis of oxazolidine derivatives was conducted following a previously established procedure.[10,15,16] Initially, 1,1,2-trimethylbenz[*e*]indole (A, 20 mmol, 4.2 g) was dissolved in 30 mL of 2-butanone. A solution of 2-bromoethanol (25 mmol, 1.8 mL in 10 mL of 2-butanone) was then slowly added dropwise at room temperature. The mixture was then refluxed under a nitrogen atmosphere at 80 °C for 48 hours, producing light pink precipitates, as illustrated in Scheme S1 (ESI†). The precipitates (B) were collected by filtration and washed three times with acetone, yielding white solids with a reaction efficiency of 60–70%. In the subsequent step, 10 mmol of B (3.35 g) was dissolved in 20 mL of ethanol, and a solution containing 4-hydroxybenzaldehyde (20 mmol, 2.45 g) and 4-(dimethylamino) benzaldehyde (20 mmol, 2.98 g) in 10 mL of ethanol was added. The mixture was then refluxed under a nitrogen atmosphere for an additional 48 hours. After cooling to room temperature, the orange (in the case of OX-OH) and purple (in the case of OX-NM) products were filtered and washed three times with 5 mL of cold ethanol, resulting in the oxazolidine derivatives C (OX-OH) and D (OX-NM). Their chemical structures were verified by ^{1}HNMR analysis using d_6-DMSO as the solvent, with the corresponding spectra presented in Fig. S1.†

2.4. Preparation of nanofibers by electrospinning

Nanofibers were prepared by dissolving the oxazolidine dye (3 wt%) into a copolymer solution of DMF : CH_2Cl_2 (1 : 3, v/v) at a predetermined concentration (60 mg mL^{-1} PM-NFs, 38 mg mL^{-1} PMHE-NFs, 24.2 mg mL^{-1} PMSO-NFs, and 37.5 mg mL^{-1} PMDM-NFs; NFs refers to nanofibers), allowing the mixture to dissolve at ambient temperature for 24 hours. The concentration of the polymer solution plays a crucial role in the electrospinning process, impacting the final nanofiber morphology. The copolymer solutions were electrospun onto glass and aluminum foil surfaces at a flow rate of 0.001 mL min^{-1}, with an applied voltage of 21–22 kV and a needle tip-to-collector distance of 110 mm.

3. Results and discussion

Familiarity with phenomena such as hydrochromism, solvatochromism, halochromism, and photochromism enhances the effectiveness of chemosensors in solution media. Oxazolidine derivatives exhibit these properties across various pH levels and solvents due to their unique conjugated structures.[10,39,40] Each functional group in oxazolidine contributes to specific fluorescence intensities and colors, which are influenced by the presence of electron-donating and electron-withdrawing groups in the aldehyde structures, as already observed in this study. Consequently, oxazolidine derivatives with various functional groups, including hydroxyl and tertiary amine, were synthesized as outlined in Scheme S1,† and their chemical structures were confirmed through ^{1}HNMR analysis using d_6-DMSO as the solvent (Fig. S1†). To create stimuli-responsive nanofibers, high-

Table 1 A typical procedure for the synthesis of multi-functionalized polymer nanoparticles based on PMMA by emulsion polymerization

Sample	Water (mL)	MMA (g)	HEMA (g)	DMAEMA (g)	APSA (g)	KPS (g)	$NaHCO_3$ (g)	SDS (g)	Triton X-100 (g)	Conversion (%)	Solid content (wt%)
PM-NPs	135	15	0	0	0	0.3	0.3	0.9	0.45	96 ± 1	10.52
PMDM-NPs	135	12	0	3	0	0.3	0.3	0.9	0.45	98 ± 1	10.99
PMHE-NPs	135	12	3	0	0	0.3	0.3	0.9	0.45	96 ± 1	10.62
$PMSO_3$-NPs	135	12	0	0	3	0.3	0.3	0.9	0.45	99 ± 1	11.06

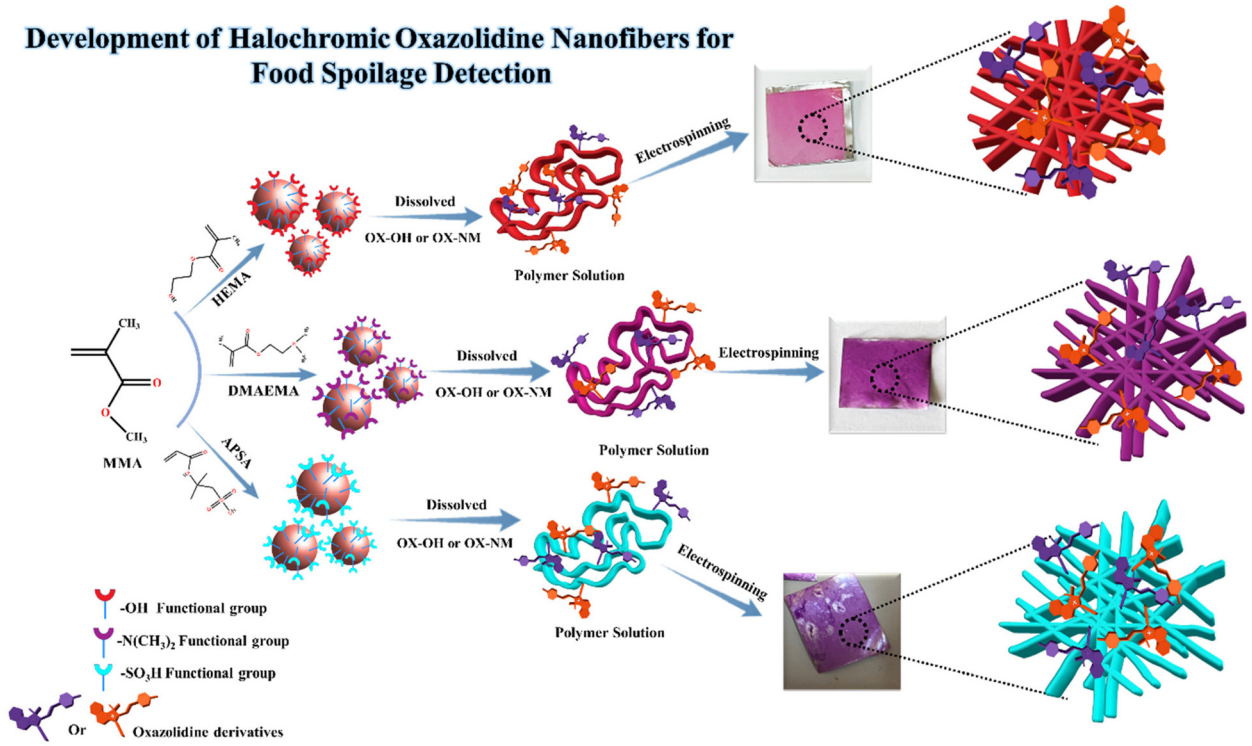

Scheme 1 A schematic illustration of the synthesis process for stimuli-chromic latex nanoparticles incorporating oxazolidine derivatives.

molecular-weight random copolymers containing hydroxyl, sulfonic acid, and tertiary amine groups were synthesized *via* emulsion copolymerization, as schematically illustrated in Scheme 1. The resulting samples were allowed to dry at room temperature, thoroughly rinsed with water to eliminate surfactants, and then dried in a vacuum oven at 50 °C for 24 hours to obtain polymer powders. These powders were analyzed using ^{1}HNMR and ATR-FTIR spectroscopy, with their chemical structures successfully confirmed by ^{1}HNMR (as shown in Fig. S2†) and ATR-FTIR (Fig. S3†). The characteristic peaks in the ^{1}HNMR spectra were clearly identified and labeled. In addition, an important application of NMR analysis in polymer characterization is the determination of molecular weight (MW) *via* end-group analysis. Based on the protocols reported elsewhere,[41,42] the molecular weights of the PM-NP and PMDM-NP samples were estimated to be ~11 413 g mol^{-1} and ~11 068 g mol^{-1}, respectively (Fig. S4 and Tables S1 and S2†). However, for the PMHE-NP and PMSO$_3$-NP samples, molecular weight determination using the present protocol was not feasible due to the complete overlap of the end-group signals with the characteristic peaks of the repeating HEMA and APSA units. The quality of the prepared polymer chains was further assessed through gel permeation chromatography (GPC) analysis. This analysis revealed a narrow molecular weight distribution for all investigated polymers, with a polydispersity index (PDI) ranging from 1.1 to 1.5. The number-average molecular weight (M_n) and average molecular weight (M_w) for all polymers were also determined using gel permeation chromatography (GPC), as shown in Fig. S2.† The M_w values estimated for PM-NPs and PMDM-NPs using GPC were approximately 10 551 g mol^{-1} and 8936 g mol^{-1}, respectively. Notably, the GPC-derived M_w values for both PM-NPs and PMDM-NPs are to some extent different but still remain in acceptable agreement with those estimated using ^{1}H-NMR, taking into account the experimental errors associated with both methods.

3.1. Investigation of the morphology and surface area of nanofibers

One key factor in controlling the size and morphology of copolymer nanoparticles is the presence of functional groups within the copolymer structure.[43,44] In this study, hydroxyl, sulfonic acid, and tertiary amine functional groups were incorporated into the copolymers, and their particle sizes were analyzed using dynamic light scattering (DLS) and field emission scanning electron microscopy (FE-SEM), as illustrated in Fig. S5 and S6,† respectively. After synthesizing the multi-functionalized copolymer nanoparticles, these samples were utilized to prepare copolymer solutions in a DMF/CH_2Cl_2 (30 : 70) mixture and subsequently electrospun to produce nanofibers. The morphology and size of these nanofibers are influenced by several factors, including the solvent type, solution concentration and viscosity, polymer molecular weight, electrical field voltage, and syringe flow rate.[45,46] The presence of functional groups in the nanofibers significantly impacts their morphology, as interactions between polymer chains and polar functional groups can increase viscosity, thereby affecting the distribution of fiber diameters.[43,47,48] Therefore, the main

reason for the selection of PMMA and other functional co-polymers as the main matrices in the present study is based on their suitable polarity, which ensures the effective responsiveness of oxazolidine. Additionally, its high transparency and durability offer excellent compatibility with the visual quality requirements of food packaging applications. It is important to emphasize that the functional groups in the functionalized nanofibers have significantly higher accessibility compared to their corresponding dense and bulk polymers. Consequently, the morphology of the nanofiber matrix is likely to enhance the optical properties of oxazolidine, including light absorption and emission. Furthermore, we believe that the nanofiber structure of the employed matrices can create a suitable microenvironment that improves the stability of oxazolidine within the polymer matrix, ultimately leading to prolonged photostability and enhanced performance in the prepared films. Therefore, in this study, we chose to investigate functionalized polar nanofibers as matrices for constructing novel halochromic oxazolidine nanofibers.

FESEM images presented in Fig. 1 were utilized to examine the morphology of the nanofibers. The electrospun nanofibers exhibited well-defined morphology and structure, smooth surfaces, and uniform diameters with a narrow size distribution. The average diameters were below 550 nm. FESEM images and analyses conducted using ImageJ® software revealed the following diameter distributions: PM-NFs had an average diameter of 462 ± 91 nm, PMDM-NFs: 537 ± 84 nm, PMHE-NFs: 143 ± 33 nm, and PMSO-NFs: 375 ± 86 nm. Notably, PMHE-NFs, with a concentration of 38 mg mL^{-1}, exhibited the smallest average diameter and the most uniform distribution. The impact of functional groups on fiber diameter is tied to their effects on solubility, viscosity, and intermolecular interactions within the polymer solution. The PMDM-NFs, which contain tertiary amine groups, demonstrate increased fiber diameters due to enhanced intermolecular interactions, such as hydrogen bonding or ionic interactions, which elevate solution viscosity. These interactions can also result in uneven charge distribution on the polymer jet during electrospinning, contributing to the formation of thicker fibers. The PMSO-NFs, which possess sulfonic acid groups, exhibit similar effects. The high polarity of sulfonic acid can induce strong ionic interactions in polar environments, increasing the viscosity and potentially leading to thicker fibers. Despite having a lower concentration (24.2 mg mL^{-1}) compared to PMDM-NFs (37.5 mg mL^{-1}), the negative surface charge on PMSO-NFs can cause repulsion between polymer chains, necessitating a lower concentration for optimal viscosity. The PMHE-NFs, which contain hydroxyl groups, afford finer fibers. Hydroxyl groups form weaker hydrogen bonds compared to sulfonic acid and amine groups, resulting in lower viscosity and improved fiber stretching. This, along with enhanced solubility in polar solvents, contributes to the production of finer and more uniform fibers. Overall, controlling the functional groups allows for precise tuning of the fiber diameter, surface chemistry, and internal structure, thereby optimizing the electrospinning process and the properties of the resulting nanofibers. The small diameter and high surface area of these multifunctional nanofibers are expected to enhance their stimuli-chromic properties and fluorescence emission, even with minimal oxazolidine content. This enhancement is attributed to increased light absorption and reduced light reflection, combined with a high concentration of oxazolidine molecules on the nanofiber surfaces.

The Brunauer–Emmett–Teller (BET) calculations, which measure the specific surface area using N_2 sorption analysis, reveal that nanofibers typically possess a suitable surface area due to their small diameter and large aspect ratio. Among the samples analyzed, PMHE-NFs, with a smaller diameter of 143 nm, exhibit the highest surface area of 14.78 $m^2\ g^{-1}$. In contrast, PMDM-NFs demonstrate a surface area of 11.13 $m^2\ g^{-1}$, which is higher compared to PM-NFs with a surface area of 7.5 $m^2\ g^{-1}$. The lower surface area of PM-NFs compared to PMDM-NFs can likely be attributed to the higher packing density of polymeric nanoparticles and the significantly lower inter-particle porosity in the former. This results in reduced space for N_2 adsorption. This is an interesting finding, as it clearly shows that the packing properties of the indicated polymeric nanoparticles did not change remarkably during the preparation of the respective nanofibers, a phenomenon that can be clearly understood by examining the FESEM images of these materials (Fig. S6† and Fig. 1). Although we do not have a precise reason for this observation, the presence of functional groups, such as tertiary amines, may partially contribute to this effect. With this explanation, the low surface area of PMSO-NFs (5.39 $m^2\ g^{-1}$) may also be interpreted in a similar manner. However, in the case of PMSO-NFs, it is important to emphasize that the hydrogen bonding between sulfonic acid functional groups can intensify the degree of aggregation, which in turn reduces the effective surface area available for gas adsorption. The adsorption isotherm diagrams and BET analysis for all nanofibers are shown in Fig. S7.† After incorporating the oxazolidine dye into the nanofiber matrix, atomic force microscopy (AFM) was utilized to confirm that the doping process did not alter the morphology of the nanofibers. The results, illustrated in Fig. S8,† demonstrate that the structure of the nanofibers remained consistent.

Fluorescence microscopy is a powerful technique for visualizing electrospun nanofibers, enabling a detailed examination of their structure and properties at the nanoscale. The fluorescent oxazolidine derivative molecules were uniformly dissolved throughout the electrospun fibers, as shown in Fig. S9.† Fluorescence images of the nanofibers confirmed their alignment and morphological features.

The chemical composition of a surface strongly influences its hydrophilicity and hydrophobicity. The topography of the surface nanofibers is an important parameter for evaluating surface quality.[44,49] Evaluation of the contact angle (Fig. S10 (A–D)†) and three-dimensional surface roughness (Fig. S10(A′–D′)†) of the stimuli-chromic nanofibers showed that for hydrophilic surfaces, decreased roughness results in a decreased contact angle, while for hydrophobic surfaces, increased roughness leads to an increased contact angle.

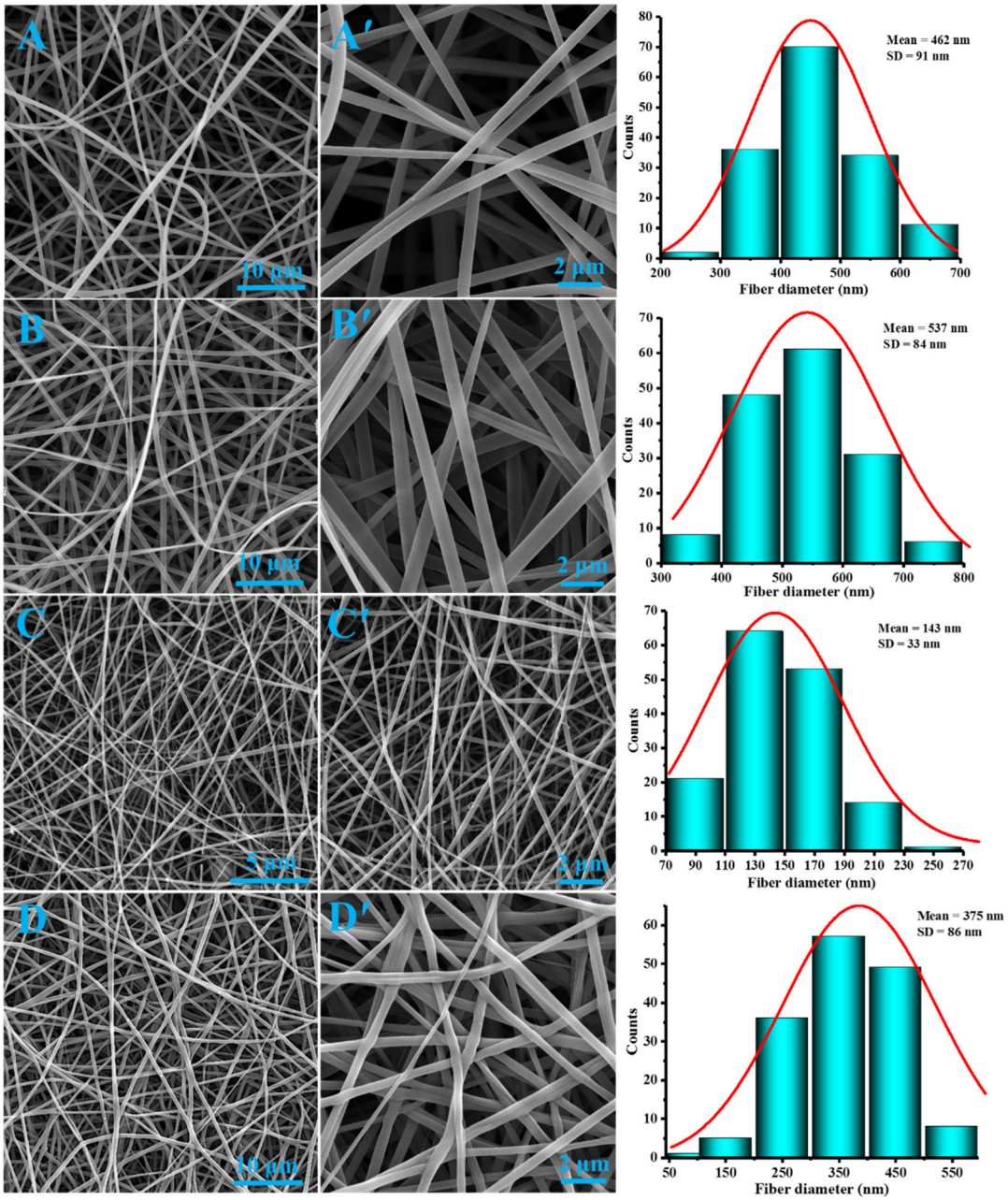

Fig. 1 FESEM images of the nanofibrous coatings prepared by electrospinning of copolymer solutions and fiber diameter distributions with the average diameter of optimal nanofibers (data are expressed as mean ± standard deviation), collected from (A and A′) PM-NFs, (B and B′) PMDM-NFs, (C and C′) PMHE-NFs, and (D and D′) PMSO-NFs.

3.2. The impact of local polarity on optical characteristics of oxazolidine derivatives

To investigate the interaction between the oxazolidine dye and the nanofiber matrix, we analyzed the optical properties of the samples using solid-state UV-Vis and fluorescence spectroscopy, with the results displayed in Fig. S11.† Overall, the observed fluorescence behaviors are primarily influenced by the polarity of the media and the copolymer matrix by oxazolidine isomerization, as schematically illustrated in Scheme S2,† which are closely related to the solvatochromic phenomenon.

3.3. Investigation of the pH responsivity of stimuli-chromic nanofibers

Oxazolidine derivatives exhibit a pronounced pH-dependent response. Their interaction with the surrounding medium demonstrates solvatochromic behavior, wherein the color change is associated with the alterations in the molecule's electronic structure. These changes influence the compound's light absorption and emission properties. The halochromic color transition of oxazolidine is generally reversible, enabling the material to revert to its original color once the pH returns

to a neutral state. Before investigating the pH-responsive behavior of nanofibers containing oxazolidine, we examined oxazolidine derivative solutions under different pH conditions and in the presence of different aromatic and aliphatic amines to assess the impact of their incorporation into the nanofiber matrix. The results, presented in Fig. S12 (oxazolidine solutions) and Fig. S13† (oxazolidine nanofibers), demonstrate that the optical properties were preserved within the nanofiber matrix across a wide pH range (1–14). The amine-responsive behavior of oxazolidine derivative solutions was investigated in response to both aliphatic and aromatic amines, as alkaline vapors (amine products) are produced by some foods, such as fish, and the results are presented in Fig. S14 and S15† under UV light and visible light. Aromatic amines enhance fluorescence intensity and UV-Vis absorption by stabilizing the excited state through conjugation, while aliphatic amines lack this effect. However, the presence of hydroxyl-containing oxazolidine derivatives can disrupt this conjugation, reducing the overall stabilization.

The matrix plays a crucial role in the halochromic behavior of nanofibers by adsorbing acidic or basic vapors onto their surface. This adsorption enhances the interaction between oxazolidine molecules and the vapors produced by food spoilage, thereby facilitating more effective spoilage detection. In this context, the optical properties of copolymer nanofibers exposed in acidic and basic media were demonstrated using solid-state UV-Vis and fluorescence spectroscopy, which are illustrated in Fig. 2 and 3. Fig. 2A and A′ present the solid-state UV-Vis and fluorescence spectra of the PM-NFs(OX-OH) sample, respectively, where a slight pH responsivity was observed. In the PMDM-NFs(OX-OH) + HCl sample, the blue shift in the UV-Vis spectra (Fig. 2B) was observed, which is related to the protonation of OX-OH in acidic media, as well as the pH responsivity of DMAEMA within this matrix. The fluorescence emission of this sample (Fig. 2B′) is quite decreased in acidic media due to the presence of fluorescence oxazolidine dyes that are pH-sensitive. Under acidic conditions, the dye's fluorescence may be quenched due to protonation of phenolate hydroxyl sites, potentially leading to the dye's emission spectrum or even complete quenching if the acidic environment significantly affects the dye's excited state. On the other hand, in acidic media, the amine group in DMAEMA becomes protonated, converting the neutral amine group ($-NR_2$) into a positively charged ammonium ion ($-NR_2H^+$). This protonation alters the electronic environment of the nanofiber, which can influence the fluorescence properties of the dye. In the PMHE-NFs(OX-OH) nanofiber, a red shift in the UV-Vis spectra (Fig. 2C) was observed in basic media, indicating that the electronic transitions in the dye occur at lower energy levels. This shift is consistent with enhanced conjugation and electron delocalization within the dye structure in a basic environment. The basic conditions can alter the electronic structure of the oxazolidine dye, resulting in changes to its absorption characteristics. The red shift indicates that the oxazolidine dye absorbs light at longer wavelengths due to the stabilization of its excited state and increased electron delocalization. The fluorescence intensity of PMHE-NFs(OX-OH) in acidic media was increased according to Fig. 2C′. In basic media, the hydroxyl groups in both oxazolidine and HEMA may undergo deprotonation, leading to the generation of negatively charged oxygen species. Deprotonation can enhance the electron density across the structure of the dye, resulting in improved electronic interactions and delocalization through conjugation. The PMSO-NFs(OX-OH) under basic conditions show a red shift in UV-Vis spectra (Fig. 2D). In fact, the sulfonic acid groups ($-SO_3H$) can lose a proton, transforming into negatively charged sulfonate groups ($-SO_3^-$). This deprotonation increases the overall negative charge in the nanofiber matrix, which can influence the electronic environment of the oxazolidine dye. The negative charge on the sulfonate groups can enhance electrostatic interactions with the dye, potentially leading to a more stabilized excited state. This stabilization can increase the fluorescence intensity as shown in Fig. 2D′. The CIE 1931 colorimetric diagram in Fig. 2A″–D″ reveals a remarkable color shift for PMSO-NFs(OX-OH) under basic conditions and PMDM-NFs(OX-OH) in acidic media, confirming the results derived from UV and fluorescence spectroscopy.

Therefore, the optical properties of fluorescent nanofibers result from a complex interplay among the functional groups present in the matrix and dye, the pH of the environment, and the solvatochromic behavior of the dye. Functional groups in the matrix can modify the electronic environment of the dye through hydrogen bonding, electrostatic interactions, and changes in rigidity. The pH of the medium affects protonation states, leading to variations in the fluorescence intensity and wavelength. Solvatochromism further modulates the optical properties based on the polarity of the environment, contributing to red or blue shifts in the spectra. Altogether, these factors determine the overall optical behavior of the stimulichromic nanofibers.

In the next stage, we have thoroughly explored and investigated the use of oxazolidine derivatives with tertiary amine functional groups (OX-NM) incorporated into copolymer nanofibers to assess their pH responsiveness in various media. Fig. 3A and A′ display the solid-state UV-Vis and fluorescence spectra for the PM-NFs(OX-NM) sample, respectively, where the slight pH responsivity was observed. As illustrated in Fig. 3B, the protonation of tertiary amine groups in both the dye and matrix in the PMDM-NFs(OX-NM) sample in acidic media results in a decrease in fluorescence intensity (Fig. 3B′) due to quenching mechanisms, as well as a blue shift in the UV-Vis spectra, which is attributed to an increased energy gap and reduced conjugation. The changes induced by protonation in the electronic environment and interactions within the nanofiber matrix also contribute to these observed optical behaviors. In addition, a decrease in intensity was noted in the UV-Vis spectra for the PMDM-NFs (OX-NM) sample in basic media. In this environment, the absence of protonation in the tertiary amine groups of both the dye and the matrix leads to diminished electronic conjugation and weaker dye–matrix interactions. These factors contribute to a decrease in light absorption efficiency, resulting in a lower intensity of the UV-Vis spectra. A slight responsivity was observed in

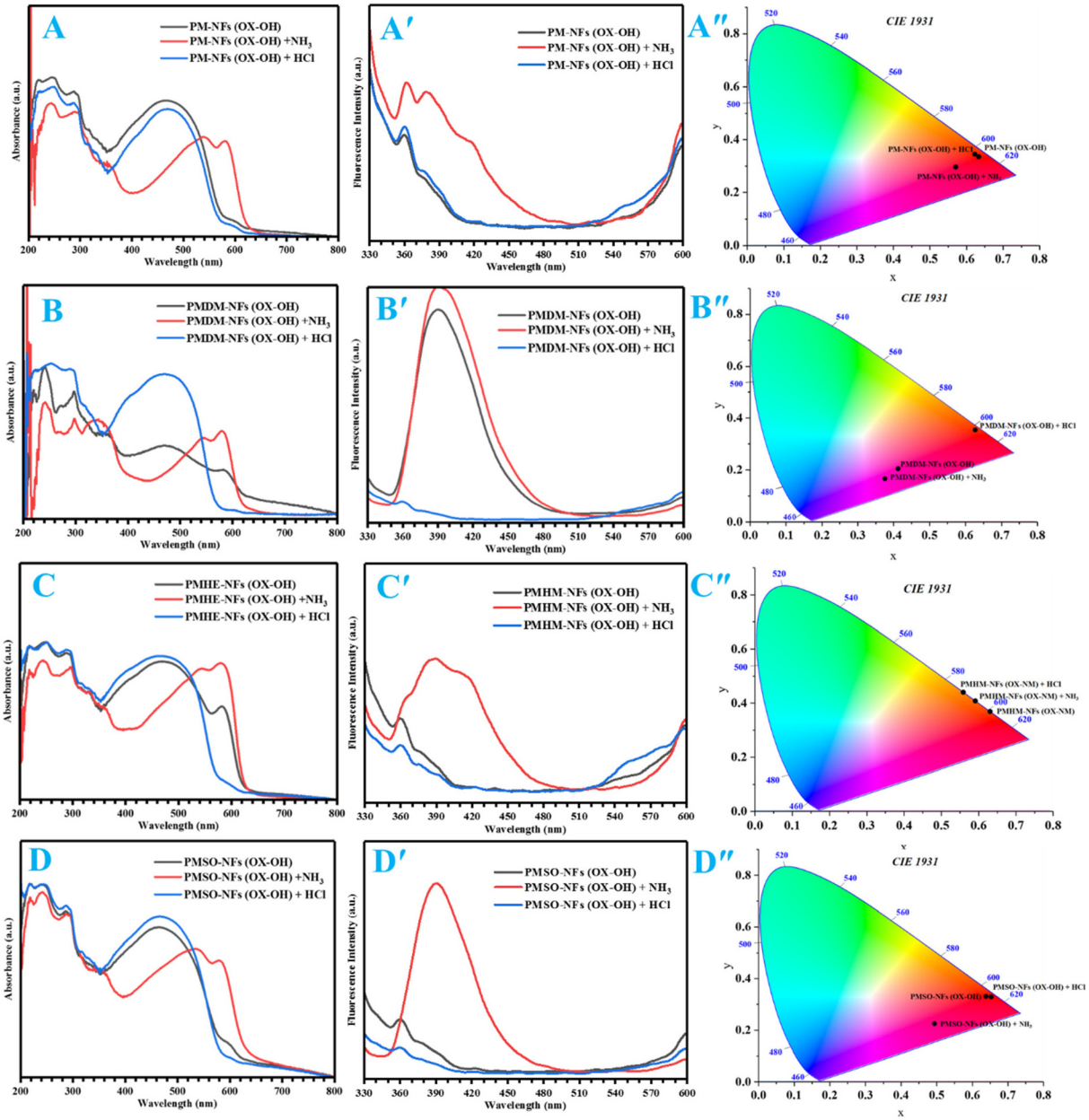

Fig. 2 (A and D) Solid UV–Vis, (A′–D′) solid fluorescence excited at 310 nm, and (A″–D″) the CIE colorimetric diagram of the pH-responsive photoluminescent nanofibers incorporated into the OX-OH dye.

both the UV-Vis spectra (Fig. 3C and D) and fluorescence spectra (Fig. 3C′ and D′) for the PMHE-NFs(OX-NM) and PMSO-NFs (OX-NM) samples, respectively. The CIE colorimetric diagram in Fig. 3A″, B″, C″ and D″ did not exhibit a notable color shift for any of the samples. Therefore, based on the observed results, we can conclude the significance of the functional groups of the dyes and their interactions with functional groups of the matrix and media. This interaction accounts for the differing results observed from two distinct functional groups of oxazolidine in response to pH responsivity of the media.

The halochromic fibers are typically manifested as fluorescence quenching, bathochromic shifts (red shifts), hypsochromic shifts (blue shift), hyperchromic effects, and hypochromic effects. To further examine the response to acidic and basic conditions, we investigated the Stokes shift parameter, which can be considered strong evidence for examining the impact of the medium on the optical properties of oxazolidine, commonly known for its solvatochromism. Important parameters such as $\lambda_{max(abs)}$, $\lambda_{max(em)}$, and the Stokes shift were extracted from UV-Vis and fluorescence spectra, and the results are presented in Table S1.†

Fig. 4 illustrates the visual results of solid-state solvatochromism and halochromism in stimuli-chromic nanofibers under UV (365 nm) and visible light. These obser-

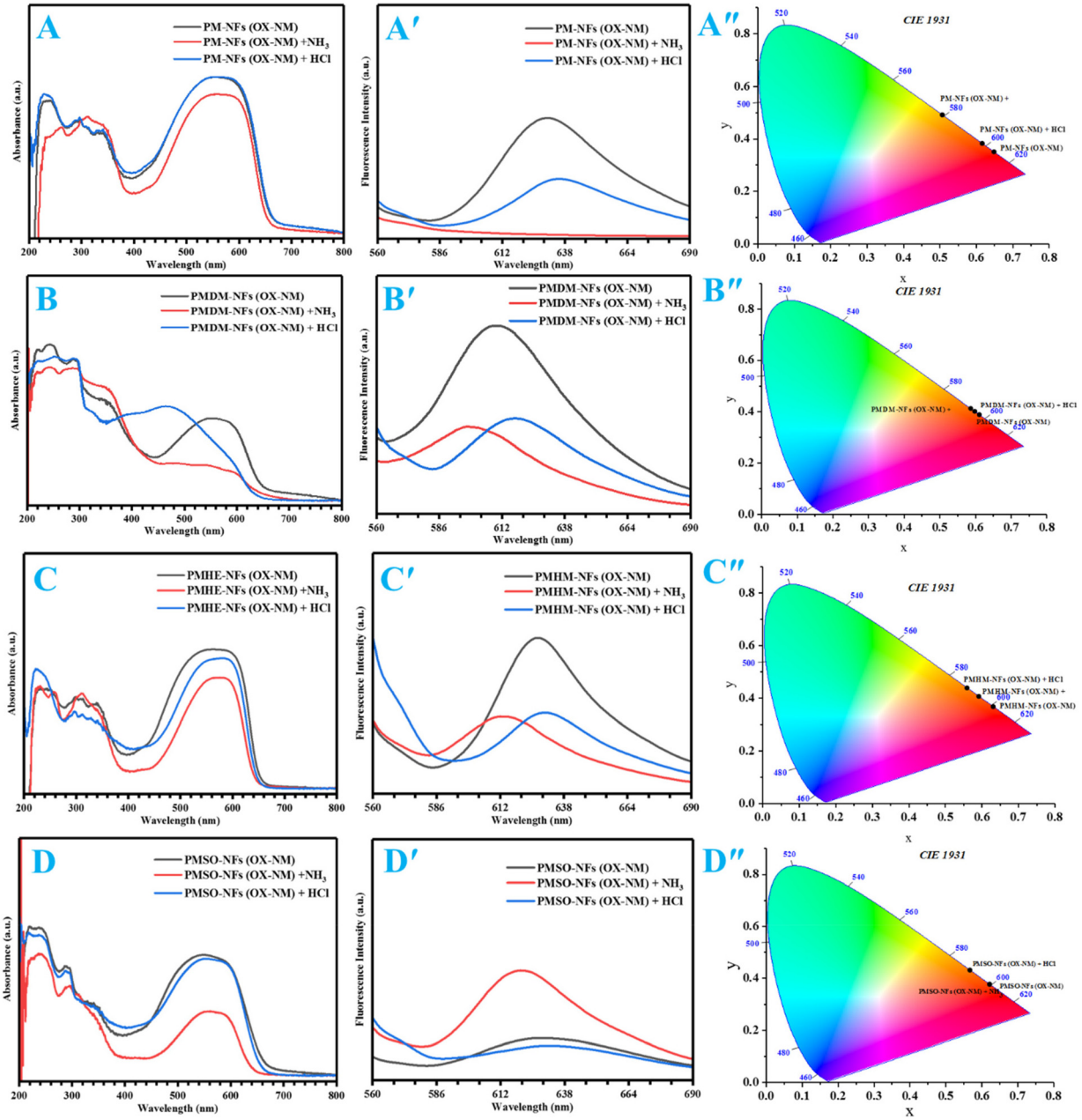

Fig. 3 (A–D) Solid UV–Vis, (A′–D′) solid fluorescence excited at 540 nm, and (A″–D″) the CIE colorimetric diagram of the pH-responsive photoluminescent nanofibers incorporated into the OX-NM dye.

vations corroborate the findings from UV-Vis and fluorescence spectroscopy, providing compelling evidence for the fluorimetric and colorimetric behaviors of the developed intelligent nanofibers. This supports their potential application in detecting food spoilage through exposure to acidic and basic environments. Movie 1† demonstrates the colorimetric and fluorimetric behaviors of the PMSO-NFs (OX-OH) in response to ammonia where the color changes from yellow to peach. The change in color and fluorescence in response to ammonia is demonstrated in Movie 2† for PMDM-NFs (OX-NM).

One of the novel interesting features of these tags is their reusability and reversibility, allowing them to be employed multiple times without any decrease in optical properties. The reusability of halochromic nanofibers is presented in Fig. S16.†

3.4. Photoluminescent intelligent nanofiber indicators for detection of acidic and basic food spoilage

The outcomes of this study revealed the substantial applicability of photoluminescent pH-responsive nanofiber samples for monitoring food spoilage. Foods that undergo spoilage processes involving protein degradation, such as dairy products,

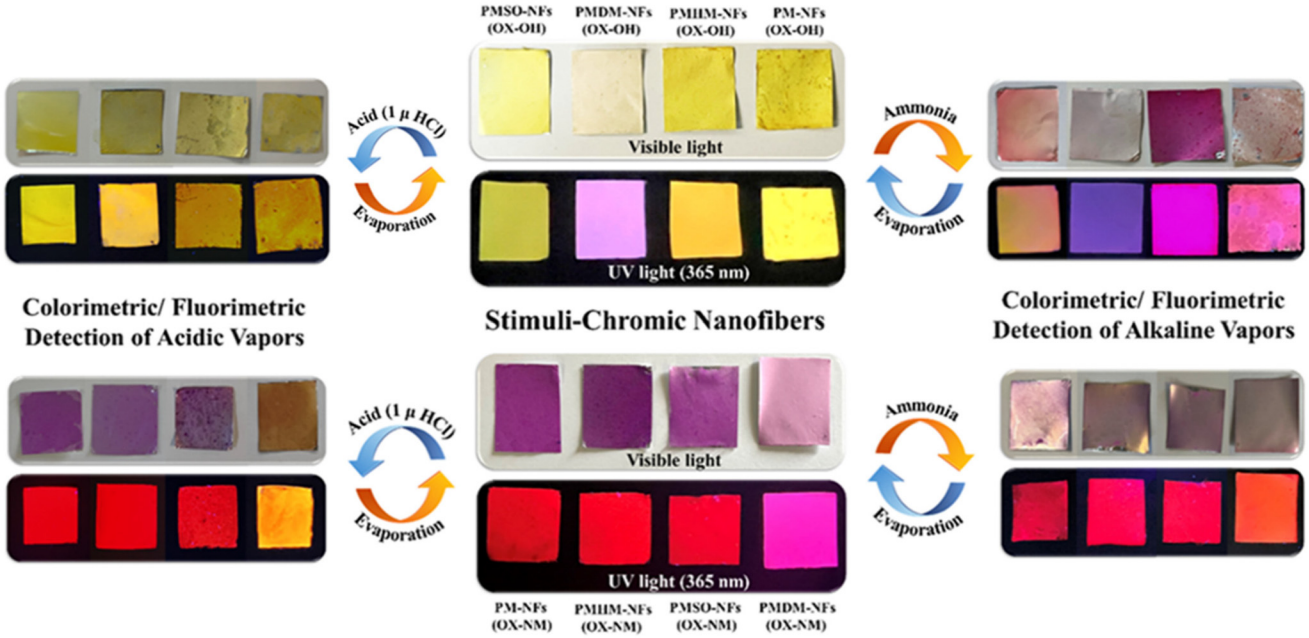

Fig. 4 The photoluminescent nanofiber images under UV (365 nm) and visible light.

can release both basic or acidic vapors. In fact, bacterial decomposition and oxidation processes in food materials lead to spoilage, generating these vapors. Oxazolidine was incorporated as a pH-responsive fluorescent dye into a nanofiber matrix with varying functional groups. Upon interaction with the surrounding environment and the matrix, oxazolidine induced distinct signals, including visible color changes, alterations in fluorescence intensity, or even fluorescence quenching. These properties enable the nanofibers to function as intelligent, portable tags that can be applied in food packaging, allowing consumers and producers to easily determine the freshness or spoilage of the food product. In this study, four different food products (lamb meat, chicken meat, fish, and milk) were utilized to monitor their spoilage processes using photoluminescence nanofiber tags. Milk, as a dairy product, produces acidic vapors during the spoilage process. According to previous reports,[5,50] a pH value below 6.6 indicates milk spoilage due to bacterial activity and lactic acid formation. We investigated the kinetics of pH changes over time during the milk spoilage process, with the results shown in Fig. S17.† The pH of the milk decreased from 6.78 on day 0 to 5.54 on day 11. This decrease is attributed to the progressive release of lactic acid as the milk spoils over time. To develop a sensor for detecting acidity in milk products, PMDM-NFs(OX-OH) and PMDM-NFs(OX-NM) nanofiber tags were placed on the caps of milk bottles. These tags were used to detect spoilage by detecting acidic vapors emitted from spoiled milk. The relatively porous structure of the nanofibers functions as a membrane for the adsorption of acidic vapors, aiding in the development of a chemosensor for the visual detection of food spoilage. The photoluminescent nanofiber indicators were analyzed using solid UV-Vis (Fig. 5A and B) and solid fluorescence (Fig. 5A′ and B′) spectroscopy to assess their optical properties before and after milk spoilage. The results indicated that for both acidic milk spoilage tags, a remarkable peak intensity within the range of 400–600 nm in UV-Vis spectra appeared after three days, indicating maximum milk spoilage on day 3. Subsequently, the concentration of acid vapors decreased, resulting in a reduction of absorbance intensity. In addition, the rate of spoilage exhibited a noticeable decline with a steep drop in the fluorescence spectra after the third day.

Fish naturally contain a compound called trimethylamine *N*-oxide (TMAO), which enables them to survive in cold and high-pressure environments. During spoilage, bacteria reduce TMAO to trimethylamine (TMA), a compound characterized by a strong, fishy odor and basic properties. Therefore, the PMDM-NFs(OX-OH) and the PMDM-NFs(OX-NM) were employed as basic responsive tags to monitor fish spoilage. The optical properties of these tags were analyzed using solid UV–Vis (Fig. 5C and D) and solid fluorescence (Fig. 5C′ and D′) spectroscopy to evaluate their performance during the spoilage process of fish. The results revealed that the spoilage process of fish began on the first day, with maximum deterioration occurring on day 2. A sharp decrease was observed in fluorescence intensity on the second day. It appears that the PMSO-NFs(OX-OH) tag is slightly more sensitive than the PMDM-NFs(OX-NM) tag, as it detected the fish earlier.

On the other hand, it is known that lamb meat, as a protein-rich product, produces acidic vapors during the spoilage process due to the breakdown of proteins and fats by microbial metabolism and enzymatic processes. This breakdown leads to the formation of acidic byproducts such as lactic acid, acetic acid, and other organic acids. Therefore, the PMDM-NFs(OX-OH) and the PMDM-NFs(OX-NM) were utilized as acid-responsive tags to investigate the spoilage process of

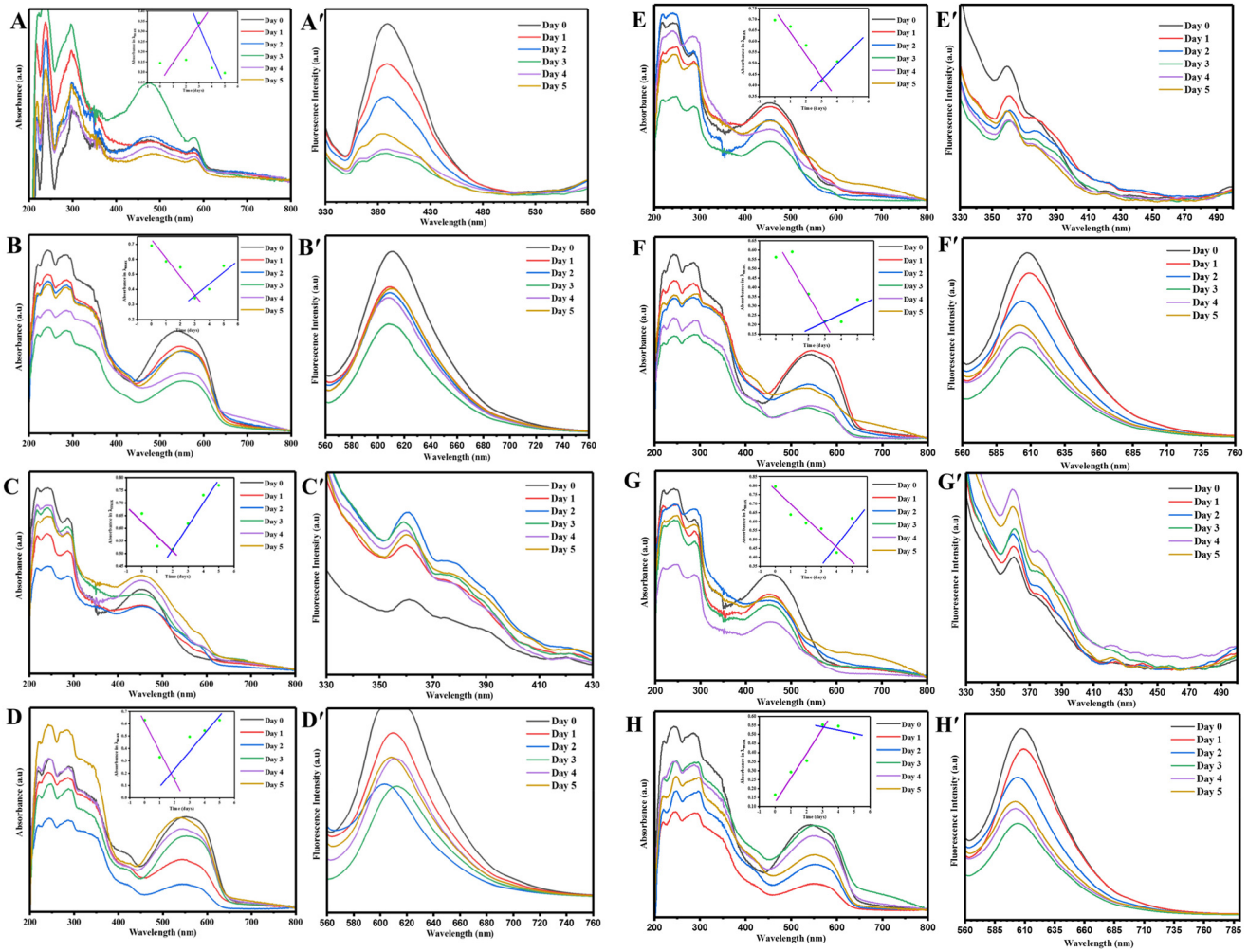

Fig. 5 (A–H) Solid UV–Vis and (A′–H′) solid fluorescence spectra of the photoluminescent smart nanofiber indicator for food spoilage collected from (A and A′) PMDM-NFs(OX-OH) in acidic milk spoilage, (B and B′) PMDM-NFs(OX-NM) in acidic milk spoilage, (C and C′) PMSO-NFs(OX-OH) in basic fish spoilage, (D and D′) PMDM-NFs(OX-NM) in basic fish spoilage, (E and E′) PMSO-NFs(OX-OH) in acidic lamb meat spoilage, (F and F′) PMDM-NFs(OX-NM) in acidic lamb meat spoilage, (G and G′) PMSO-NFs(OX-OH) in basic chicken spoilage, and (H and H′) PMDM-NFs(OX-NM) in basic chicken spoilage.

lamb meat by evaluating their optical behavior through solid UV–Vis (Fig. 5E and F) and solid fluorescence (Fig. 5E′ and F′) spectroscopy. The analysis revealed that the spoilage process in meat began on the second day, with maximum spoilage observed on the third day for both types of intelligent tags. A significant decline in fluorescence intensity was then noted after the third day.

Chicken meat produced basic vapors during proteolysis of spoilage, resulting in the release of amino acids. One of the key basic compounds generated during the spoilage of chicken meat is ammonia. Ammonia is formed through the deamination of amino acids, where the amino group ($-NH_2$) is removed and converted into ammonia. Considering the fact that the PMSO-NFs(OX-OH) and PMDM-NFs(OX-NM) tags are responsive to basic environments, they were reasonably applied for detection of chicken spoilage, during which their optical properties were investigated by solid UV–Vis (Fig. 5G and H) and solid fluorescence (Fig. 5G′ and H′) spectroscopy. The outcomes of the UV-Vis spectra indicated that the PMSO-NFs (OX-OH) tags detected the chicken spoilage on day 3, while the PMDM-NFs(OX-NM) tags responded on day 4, indicating its lower sensitivity. Furthermore, the spoilage rate exhibited a substantial increase after the third day for the PMSO-NFs (OX-OH) tag, while a reduction in fluorescence intensity was noted on the fourth day for the PMDM-NFs(OX-NM) tags.

Each of the prepared smart tags is capable of detecting various types of food spoilage by signaling through changes in fluorescence intensity, color shifts, discoloration, or even fluorescence quenching. These responses are driven by molecular interactions among the functional groups of the oxazolidine dye, the functional groups of the matrix, and the pH of the surrounding medium, demonstrating solvatochromic behavior. It is essential to highlight that the concentrations of acids or bases in actual food samples are lower than those used in the

controlled experiments depicted in Fig. 2, 3, and 4, where samples were directly exposed to these conditions.

Consistent with the findings from solid-state UV-Vis and fluorescence spectra (Fig. 5) for acidic and basic foods, the halochromic behavior of intelligent tags containing PMDM-NFs(OX-NM), PMDM-NFs(OX-OH), and PMSO-NFs(OX-OH) was evaluated across various food spoilages including milk, fish, lamb meat, and chicken meat, as illustrated in Fig. 6. Halochromic nano-

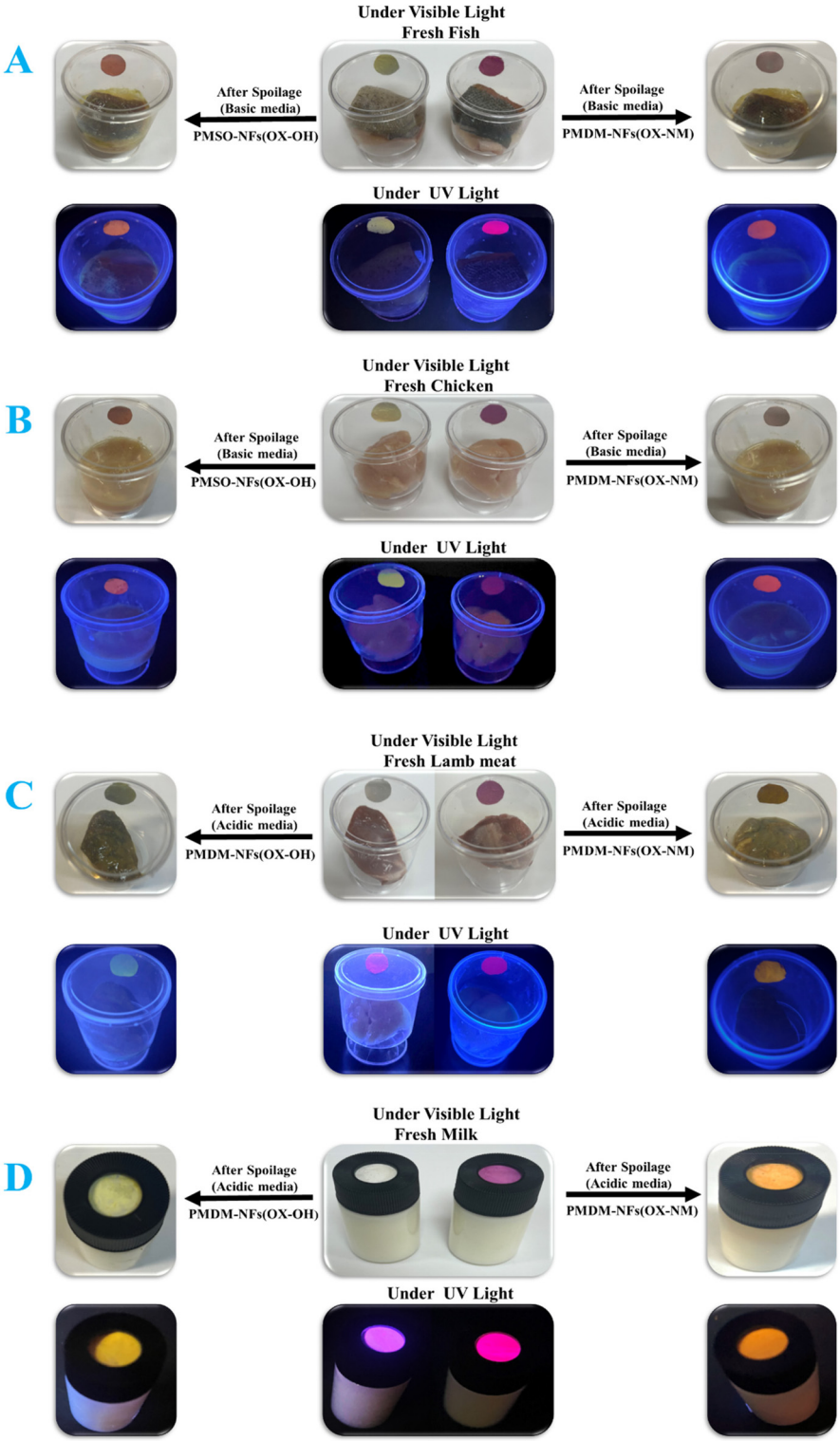

Fig. 6 Stimuli-chromic nanofiber indicator for detection of acidic and basic food spoilage for (A) fish, (B) chicken meat, (C) lamb meat, and (D) milk.

fiber tags were placed in fresh food dishes or on milk bottle caps, with spoilage being monitored visually under UV and visible light over a 5-day period at room temperature at about 27–30 °C. All the intelligent tags clearly demonstrated colorimetric and fluorimetric behavior in response to acidic or basic conditions, exhibiting colorless states, color changes, fluorescence quenching, and variations in fluorescence intensity. As previously mentioned, during the spoilage of fish and chicken, basic vapors are produced. To detect these vapors, PMDM-NFs (OX-NM) and PMSO-NFs(OX-OH) were employed as base-responsive tags. The PMDM-NFs(OX-NM) exhibited both colorimetric and fluorimetric responses throughout the spoilage process, specifically changing the color from purple to nearly colorless under visible light and from light pink to orange under UV light irradiation, as visually demonstrated in Fig. 6A and B. The PMSO-NFs(OX-OH) nanofibers displayed a color change from yellow to peach pink under visible light and from yellow to peach under UV light irradiation, as shown in Fig. 6A and B. Upon spoilage of lamb meat and milk, acidic vapors were released, leading to adsorption by the PMDM-NFs(OX-NM) and PMDM-NFs(OX-OH) nanofibers. This resulted in noticeable changes in both color and fluorescence. The PMDM-NFs (OX-NM) nanofibers shifted from a purple hue to amber (yellow-orange) under visible light, with fluorescence transitioning from pink to yellow. Furthermore, the fluorescence of PMDM-NFs (OX-NM) altered from light pink to orange. Meanwhile, the light yellow PMDM-NFs(OX-OH) nanofibers turned yellow under visible light under acidic conditions, and their fluorescence shifted from lilac to yellow, as shown in Fig. 6C and D. Therefore, color changes are easily observed with the naked eye, making this an accessible and non-invasive method for consumers and manufacturers. Fluorimetric methods are more sensitive than colorimetric methods and are capable of detecting lower concentrations of spoilage compounds. Sensors that combine both colorimetric and fluorimetric responses for a more comprehensive spoilage detection system can be integrated into packaging as smart tags, responding to the accumulation of spoilage-related gases such as ammonia, sulfur compounds, or volatile organic compounds (VOCs).

4. Conclusions

A novel category of intelligent optical sensors based on halochromic nanofibers was developed through the electrospinning of PMMA copolymers containing various polar functional groups, such as tertiary amine, sulfonic acid, and hydroxyl groups. Oxazolidine derivatives with hydroxyl and amine functional groups were integrated into the nanofibers to create smart tags for the photodetection of food spoilage. The morphology and structural properties of the nanofibers were confirmed through FESEM analysis and N_2 sorption analysis, revealing average diameters of 462 ± 91 nm for PM-NFs, 537 ± 84 nm for PMDM-NFs, 143 ± 33 nm for PMHE-NFs, and 375 ± 86 nm for PMSO-NFs. The diameters of the nanofibers were influenced by their functional groups, with polar groups affecting fiber diameter distribution by altering solubility, viscosity, structural packing, and intermolecular interactions within the polymer solution. Fluorescence microscopy was employed to evaluate the fluorescence intensity of the nanofibers, confirming that the oxazolidine derivatives exhibit high emission intensity even within the nanofiber matrix. The PMSO-NFs, which possess polar sulfonic acid groups on their surface, exhibited the lowest contact angle of 55° and the smoothest surface among the samples, indicating enhanced hydrophilicity. The pH and amine responsiveness of oxazolidine derivatives were investigated. The pH responsiveness was found to be closely linked to the interactions between the functional groups of the matrix and the halochromic dye across a pH range from 1 to 14. Aromatic amines, due to their conjugation delocalization of the electronic structure, are typically more reactive and can exhibit enhanced fluorescence properties. The optical properties of the nanofibers were investigated using UV-Vis and fluorescence spectroscopy, highlighting the crucial role of polar functional groups in the interactions between oxazolidine, the nanofiber matrix, and the surrounding media. Three intelligent sensor tags were selected for detecting food spoilage: acid-responsive PMDM-NFs(OX-OH), dual-responsive (acid and base) PMDM-NFs(OX-NM), and base-responsive PMSO-NFs(OX-OH). The spoilage processes of dairy and protein foods, including milk, lamb meat, fish, and chicken meat, were studied using the developed sensor tags. The interaction of oxazolidine with the matrix and media triggered alarms in the tags, such as colorimetric or fluorimetric responses, which were monitored by UV-Vis and fluorescence spectroscopy. The intelligent pH-indicator nanofibers proved effective in detecting spoilage, showing noticeable changes after 3 days for milk, lamb meat, and chicken meat, and after 2 days for fish. All the prepared intelligent sensor tags exhibited reversible pH responsivity with high sensitivity and rapid response times, making them particularly valuable for the development of intelligent chemosensors in the food packaging industry. The developed PMDM-NFs(OX-NM) sensor, capable of simultaneously detecting both acidic and basic pH environments, thus provides dual applications in both dairy and protein packaging systems. Our results open a new avenue for the timely and accurate detection of food spoilage during packaging.

Author contributions

Bahareh Razavi: conceptualization, data curation, formal analysis, investigation, methodology, software, validation, visualization, and writing – original draft. Babak Karimi: conceptualization, funding acquisition, project administration, resources, supervision, and writing – review & editing.

Conflicts of interest

The authors declare that they have no known competing financial interests or personal relationships that could have appeared to influence the work reported in this paper.

Data availability

The data supporting the findings of this study are available from the corresponding author upon reasonable request.

Acknowledgements

The Institute for Advanced Studies in Basic Sciences (IASBS) Research Council (Grant No. G100/151/12882), the Iranian Science Elite Federation (ISEF), and the Iran National Science Foundation (INSF) are acknowledged for support of this work. B. R. greatly appreciates the financial support through the Dr. Chamran Postdoctoral Research Scholarship (Grant Number: 15/37492). B. K. thanks the Iran National Science Foundation (INSF) for granting International Chair no. 4039182 and the Alexander von Humboldt-Foundation for the prestigious Georg-Förster Award No. (Ref 3.4-1116632-IRN-GFPR), which provided partial support for this work.

References

1 M. Cvek, U. C. Paul, J. Zia, G. Mancini, V. Sedlarik and A. Athanassiou, *ACS Appl. Mater. Interfaces*, 2022, **14**, 14654–14667.
2 Z. Mohammadi and S. M. Jafari, *Adv. Colloid Interface Sci.*, 2020, **286**, 102297.
3 B. M. Oh, N. Y. Cho, E. H. Lee, S. Y. Park, H. J. Eun and J. H. Kim, *J. Hazard. Mater.*, 2024, **465**, 133150.
4 P. C. Wanniarachchi, K. G. Upul Kumarasinghe and C. Jayathilake, *Food Chem.*, 2024, **436**, 137733.
5 B. Razavi, H. Roghani-Mamaqani and M. Salami-Kalajahi, *ACS Appl. Mater. Interfaces*, 2022, **14**, 41433–41446.
6 D. Zhang, S. Yu, X. Wang, J. Huang, W. Pan, J. Zhang, B. E. Meteku and J. Zeng, *J. Hazard. Mater.*, 2022, **423**, 127160.
7 C. Cai, J. Mo, Y. Lu, N. Zhang, Z. Wu, S. Wang and S. Nie, *Nano Energy*, 2021, **83**, 105833.
8 S. Alfei, B. Marengo and G. Zuccari, *Food Res. Int.*, 2020, **137**, 109664.
9 R. R. Koshy, J. T. Koshy, S. K. Mary, S. Sadanandan, S. Jisha and L. A. Pothan, *Food Control*, 2021, **126**, 108039.
10 L. Sheng, M. Li, S. Zhu, H. Li, G. Xi, Y. G. Li, Y. Wang, Q. Li, S. Liang, K. Zhong and S. X. A. Zhang, *Nat. Commun.*, 2014, **5**, 3044.
11 V. K. Singh, R. K. Chitumalla, S. K. Ravi, Y. Zhang, Y. Xi, V. Sanjairaj, C. Zhang, J. Jang and S. C. Tan, *ACS Appl. Mater. Interfaces*, 2017, **9**, 33071–33079.
12 H. Zhao, X. Qin, L. Zhao, S. Dong, L. Gu, W. Sun, D. Wang and Y. Zheng, *ACS Appl. Mater. Interfaces*, 2020, **12**, 8952–8960.
13 Q. Chen, X. Liang, J. Du, Z. Wei, Y. M. Zhang, T. Zhang, T. Qin, W. Gao, L. Sheng and S. X. A. Zhang, *J. Mater. Chem. C*, 2019, **7**, 8045–8052.
14 T. Qin, L. Sheng and S. X. A. Zhang, *ACS Appl. Mater. Interfaces*, 2018, **10**, 40838–40843.
15 B. Razavi, H. Roghani-Mamaqani and M. Salami-Kalajahi, *Sci. Rep.*, 2022, **12**, 9412.
16 B. Razavi, H. Roghani-Mamaqani and M. Salami-Kalajahi, *Sci. Rep.*, 2022, **12**, 1079.
17 K. Pielak, F. Bondu, L. Sanguinet, V. Rodriguez, F. Castet and B. Champagne, *Dyes Pigm.*, 2019, **160**, 641–646.
18 E. Schoolaert, R. Hoogenboom and K. De Clerck, *Adv. Funct. Mater.*, 2017, **27**, 1702646.
19 A. Chinnappan, C. Baskar, S. Baskar, G. Ratheesh and S. Ramakrishna, *J. Mater. Chem. C*, 2017, **5**, 12657–12673.
20 Y.-Z. Long, M. Yu, B. Sun, C.-Z. Gu and Z. Fan, *Chem. Soc. Rev.*, 2012, **41**, 4560.
21 J. Zhang, J. Zhang, Y. Guan, X. Huang, M. Arslan, J. Shi, Z. Li, Y. Gong, M. Holmes and X. Zou, *Food Chem.*, 2022, **394**, 133439.
22 F. Mohseni-Shahri, A. Mehrzad, Z. Khoshbin, M. Sarabi-Jamab, F. Khanmohamadi and A. Verdian, *Int. J. Biol. Macromol.*, 2023, **224**, 1174–1182.
23 M. Duan, S. Yu, J. Sun, H. Jiang, J. Zhao, C. Tong, Y. Hu, J. Pang and C. Wu, *Int. J. Biol. Macromol.*, 2021, **187**, 332–340.
24 S. Forghani, H. Almasi and M. Moradi, *Innovative Food Sci. Emerging Technol.*, 2021, **73**, 102804.
25 M. Valdez, S. K. Gupta, K. Lozano and Y. Mao, *Sens. Actuators, B*, 2019, **297**, 126734.
26 L. M. Fonseca, E. J. D. Souza, M. Radünz, E. A. Gandra, E. da R. Zavareze and A. R. G. Dias, *Carbohydr. Polym.*, 2021, **252**, 117166.
27 R. Merckx, V. Dhaware, M. N. Leiske, K. De Clerck and R. Hoogenboom, *Chem. Mater.*, 2024, **36**, 9189–9206.
28 E. Schoolaert, R. Merckx, J. Becelaere, S. Rijssegem, R. Hoogenboom and K. De Clerck, *Adv. Funct. Mater.*, 2022, **32**, 2106859.
29 Q. Qi, Y. Li, X. Yan, F. Zhang, S. Jiang, J. Su, B. Xu, X. Fu, L. Sun and W. Tian, *Polym. Chem.*, 2016, **7**, 5273–5280.
30 W. Gao, T. Qin, G. Xi, L. Sheng and S. X. A. Zhang, *J. Mater. Chem. C*, 2018, **6**, 10775–10781.
31 Q. Chen, L. Sheng, J. Du, G. Xi and S. X. A. Zhang, *Chem. Commun.*, 2018, **54**, 5094–5097.
32 W. Mazi, Y. Yan, Y. Zhang, S. Xia, S. Wan, M. Tajiri, R. L. Luck and H. Liu, *J. Mater. Chem. B*, 2021, **9**, 857–863.
33 T. R. Pavase, H. Lin, Q. Shaikh, S. Hussain, Z. Li, I. Ahmed, L. Lv, L. Sun, S. B. H. Shah and M. T. Kalhoro, *Sens. Actuators, B*, 2018, **273**, 1113–1138.
34 Z. Li, J. R. Askim and K. S. Suslick, *Chem. Rev.*, 2019, **119**, 231–292.
35 F. Mazur, Z. Han, A. D. Tjandra and R. Chandrawati, *Adv. Mater.*, 2024, **36**, 2404274.
36 M. Yan, B. Wang and M. Wang, *ACS Food Sci. Technol.*, 2023, **3**, 1090–1097.
37 H. Zhang, X. Wei, M. B. Chan-Park and M. Wang, *ACS Food Sci. Technol.*, 2022, **2**, 703–711.
38 Y. Chen, G. Fu, Y. Zilberman, W. Ruan, S. K. Ameri, Y. S. Zhang, E. Miller and S. R. Sonkusale, *Food Control*, 2017, **82**, 227–232.

39 A. Abdollahi, H. Roghani-Mamaqani and B. Razavi, *Prog. Polym. Sci.*, 2019, **98**, 101149.
40 A. Abdollahi, H. Roghani-Mamaqani, B. Razavi and M. Salami-Kalajahi, *ACS Nano*, 2020, **14**, 14417–14492.
41 J. U. Izunobi and C. L. Higginbotham, *J. Chem. Educ.*, 2011, **88**, 1098–1104.
42 K. Hatada, K. Ute and M. Kashiyama, *Polym. J.*, 1990, **22**, 853–857.
43 H. M. Ibrahim and A. Klingner, *Polym. Test.*, 2020, **90**, 106647.
44 K. W. Kolewe, K. M. Dobosz, K. A. Rieger, C.-C. Chang, T. Emrick and J. D. Schiffman, *ACS Appl. Mater. Interfaces*, 2016, **8**, 27585–27593.
45 S. Kailasa, M. S. B. Reddy, M. R. Maurya, B. G. Rani, K. V. Rao and K. K. Sadasivuni, *Macromol. Mater. Eng.*, 2021, **306**, 2100410.
46 M. M. Nazemi, A. Khodabandeh and A. Hadjizadeh, *ACS Appl. Bio. Mater.*, 2022, **5**, 394–412.
47 S. A. Theron, E. Zussman and A. L. Yarin, *Polymer*, 2004, **45**, 2017–2030.
48 V. Beachley and X. Wen, *Mater. Sci. Eng., C*, 2009, **29**, 663–668.
49 H. S. Yoo, T. G. Kim and T. G. Park, *Adv. Drug Delivery Rev.*, 2009, **61**, 1033–1042.
50 A. Poghossian, H. Geissler and M. J. Schöning, *Biosens. Bioelectron.*, 2019, **140**, 111272.